

Development of dual functional converter for drive and charging power conversion for EV drive

Teja Sreenu Tadvika¹, Malligunta Kiran Kumar¹, Srungaram Ravi Teja¹, Ch. Rami Reddy^{2,3}

¹Department of Electrical and Electronics Engineering, Koneru Lakshmaiah Education Foundation, Vaddeswaram, India

²Department of Electrical and Electronics Engineering, Joginpally B R Engineering College, Hyderabad, India

³Applied Science Research Center, Applied Science Private University, Amman, Jordan

Article Info

Article history:

Received Nov 10, 2024

Revised Jan 11, 2025

Accepted Mar 1, 2025

Keywords:

Brushless direct current drive

Electric vehicles charging

Electric vehicles drive

Multi-functional converter

On-board charging

ABSTRACT

The adaptability of electric vehicle drives is primarily concerned with the size and efficiency of power conversion. This paper presents a unified power converter for the drive and charge functions of brushless direct current-based electric vehicle drives (BLDC). The symmetrical utilization of BLDC phase windings during charging operation is implemented for efficient power conversion. The unified converter operation, configuration, and control are presented. The proposed converter is simulated in the MATLAB/Simulink platform. The performance is evaluated using operational variables such as voltage, current, torque, and speed. A comparative study is presented regarding the size and efficiency of the proposed and existing drives. The proposed drive achieved 0.01 p.u. ripple in torque, 10-sec transient time for a change in speed full throttle command, and unity power factor current for charging operation, proving its robustness over the comparable drives.

This is an open access article under the [CC BY-SA](https://creativecommons.org/licenses/by-sa/4.0/) license.



Corresponding Author:

Malligunta Kiran Kumar

Department of Electrical and Electronics Engineering, Koneru Lakshmaiah Education Foundation

Green Fields, Vaddeswaram, Andhra Pradesh 522302, India

Email: kiran.malligunta@gmail.com

1. INTRODUCTION

The increasing demand for electric vehicles (EVs), hybrid EVs, and fuel-cell EVs necessitates innovative solutions for power electronic drive systems [1]. A variety of drives exist for the drive and charge functions of EVs, hybrid EVs, and other EVs [2]. The usual configurations are separate power converters for drive operation and charging operation [3], [4]. Several topologies are independently available for drive and charge functions. Soft-switched bidirectional converter for reflex charging [5]. A two-stage charging topology was developed [6] which efficiently performed the charging operation of EV battery. Among several motors available for drive operation, the brushless direct current (BLDC) motor proved efficient in terms of control, ruggedness, and torque performance [7]. The motors with up to nine phases were developed for torque performance. Several charging topologies were reviewed [8] in which single-stage, multiple-stage, multiplier-based, and multi-port charging of the EV battery were presented. Integrated charging is the further development for EV drives [9], [10] which attempted to reduce component count in the overall drive system.

The significant developments include the application of specialized materials for BLDC or other motor construction which present better torque performance [11], [12]. Improved charging and driving topologies including the application of soft-switched conversion [13] were reviewed. The interleaved conversion [14] proved suitable for high-gain applications. Also, isolated converters were found adoptable for high-gain power conversion [15] for charging low-voltage batteries from AC sources. The charging operation through gird-connected conversion was investigated [16] which adopted a unified converter for

drive and charge operations. The single-phase operation of a three-phase converter for the drive was presented [17] which is the requirement under a few extreme conditions of operation. Similarly, a phase-integrated charger [18] facilitated improved efficiency, ease of control, and reduced size and cost of drive.

On the other vertical, the efficiency of the drive is enhanced through optimal field-oriented control [18] which provides redundant states for freewheeling operation facilitating low power loss and thus causing improved efficiency. The finite element model (FEM) analysis was found to be a useful tool for analyzing better structure for efficiency [19]. The electromagnetic performance analysis [20], also made a better understanding of the rotor behavior under different operating conditions concerning efficiency parameters. The approach of dual rotor BLDC [21] established better torque performance. However, the drive's increased size and cost are this approach's primary drawbacks. The bi-directional PEV charger for vehicle-to-grid (V2G) [22] improved the utilization factor of the power converter module improving the reliability of the overall system. The combined motor drive and battery charge system [23] proved to increase the utilization index of the power converter. Another significant factor in improving the efficiency of the system was the control of the front-end converter for power factor correction [24] to achieve unity power factor current drawn from grid terminals. Also, advanced control strategies such as data-driven state of charge (SoC) estimation [25], and automatic charge control algorithms based on machine learning [26] were adopted to improve the efficiency of the onboard charge and drive systems.

These findings necessitated an effective onboard drive that performs multiple functions without additional components. With the objectives of reduced size drive, a dual-functional power converter (DFPC) is developed. The following novel contributions for the power converter in electric vehicle drive run by BLDC are made:

- Improved utilization of BLDC phase windings by utilizing these as interfacing filter inductances for battery charging operation.
- Symmetrical operation of power converter switches for effective voltage and current sharing.
- Unified drive and charge power converter causing reduced size and footprint of the drive.
- Automatic mode determination and closed-loop control of the drive.

The rest of the paper is organized as follows: Section 2 presents the topology of the power converter and a description of operating modes for drive and charging operations. Section 3 presents the control algorithm for drive and charging operation. Section 4 presents simulation results and discussion. Section 5 presents the conclusions.

2. DUAL FUNCTIONAL POWER CONVERTER FOR EV DRIVE

The unified converter topology for the drive and charging functions of BLDC-based electric vehicle traction drive is presented in Figure 1. The converter consists of eight power switches supplied from a battery source during drive operation and an AC grid during charging operation. The phase windings of three-phase BLDC are controlled by a three-phase power converter and it drives the transmission system of the electric vehicle. The power switches SW_1 – SW_6 function are functionally active during both drive and charge operations operation and SW_7 – SW_8 are functionally active during charging operation alone. The transitions required in switching for drive operation and charging operation are discussed in this section.

2.1. Drive operation

The dual functional converter enters drive mode under SW_7 and SW_8 are inactive with no gating signals provided to these switches which disconnect the AC source from the converter. The battery source excites the phase windings of BLDC in a sequence such as to generate a unidirectional torque under a magnetic field provided by a permanent magnet rotor. The sequence of transitions is depicted in Figure 2. The steady-state operation during one cycle of electromagnetic angular velocity of the motor is presented in Figure 2.

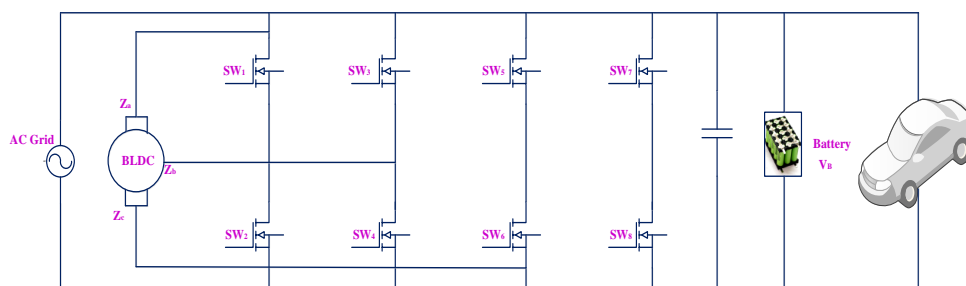


Figure 1. Dual functional power converter for BLDC-based EV drive

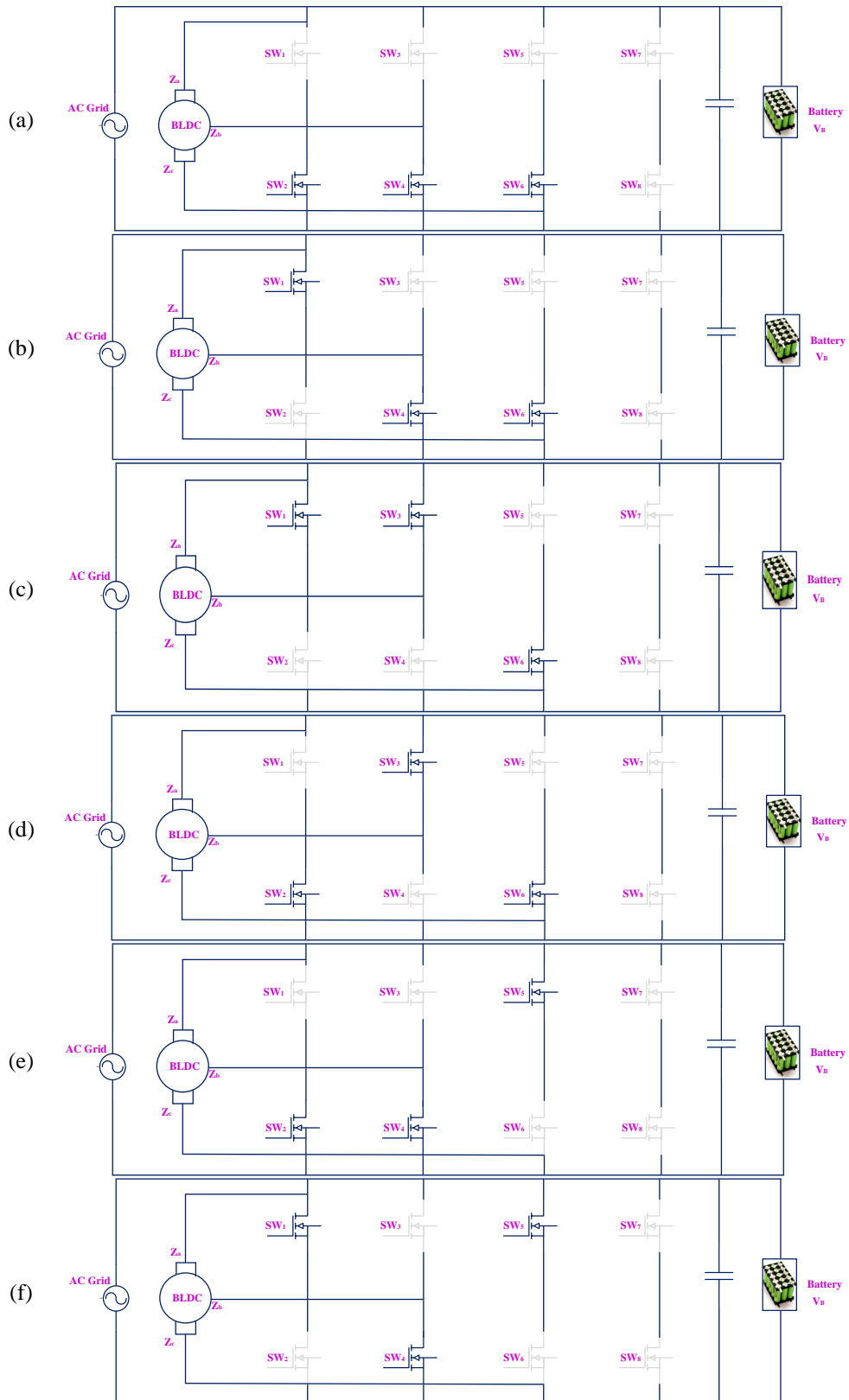


Figure 2. Switching sequence during steady state drive operation (a) zero vector along all phases, (b) phase A positive, phase B negative, and phase C negative vectors, (c) phase A positive, phase B positive, and phase C negative vectors, (d) phase A negative, phase B positive, and phase C negative vectors, (e) phase A negative, phase B negative, and phase C positive vectors, (f) phase A positive, phase B negative, and phase C positive vectors

The steady-state drive operation starting with freewheeling of BLDC phase windings owing to the previous cycle is shown in Figure 2(a). A zero vector is applied across each of the phase winding facilitating for freewheeling action which aligns the flux space vector in the axis midway between phase A and phase C. This is followed by a positive vector for phase A and negative vectors for phase B and phase C respectively as shown in Figure 2(b). This combination of vectors provides a flux space vector aligned to phase an axis. Subsequently, the flux space vector is positioned midway between phase A and phase B with the switching vectors shown in Figure 2(c). Positive vectors at phases A and b and negative vectors at phase C make flux space vectors align at the axis aligned in the center of phase A axis and phase B. Similarly, the positive vector for phase B and negative vectors for phase A and phase C respectively as shown in Figure 2(d) provides flux space vector aligned to the phase B axis. Subsequently, the flux space vector is positioned midway between phase B and phase C with the switching vectors shown in Figure 2(e). Positive vectors at phases B and C and negative vectors at phase A make flux space vector align at the axis aligned in the center of phase B axis and phase c axis. Finally, the switching combination as shown in Figure 2(f) with a positive vector at phase C and negative vectors at phase A and phase B aligns the flux space vector towards the phase C axis. The cycles repeat in the above order with a determined switching frequency to produce unidirectional torque. For reversal of the direction, the switching order is reversed from the above switching sequence.

The equivalent d-q axes reference frame vectors for voltage vectors and respective electromagnetic torque developed by the motor are given in (1).

$$\begin{cases} u_d = R_s i_d + P\psi_d - \omega_r \psi_q \\ u_q = R_s i_q + P\psi_q + \omega_r \psi_d \\ T_e = P(\psi_d i_q - \psi_q i_d) \end{cases} \quad (1)$$

Where, R_s is the stator resistance of the motor, i_d , i_q are d-axis and q-axis stator currents, respectively, ψ_d , ψ_q are permanent magnet flux linkage in the d-axis and q-axis respectively, ω_r is the rotor speed and T_e is the electromagnetic torque developed by the motor.

2.2. Charging operation

The dual functional converter enters drive mode under SW_1 and SW_2 are inactive with no gating signals provided to these switches. The charging operation involves a rectification operation followed by a voltage boost operation. The primary advantage of this converter is utilizing the locked rotor motor phase windings as charging inductors. The sequence of transitions during one cycle of input voltage is depicted in Figure 3 (see Appendix).

The switching combination as shown in Figure 3(a) determines the positive current flow through the phase inductors owing to the connection of inductors between the AC source and the battery source. The corresponding differential equations for phase currents are then obtained as provided in (2).

$$\begin{cases} Z_s \frac{di_{za}^I}{dt} = \frac{2V_{in} - V_B}{3} \\ Z_s \frac{di_{zb}^I}{dt} = \frac{2V_{in} - V_B}{3} \\ Z_s \frac{di_{zc}^I}{dt} = \frac{2V_{in} - V_B}{3} \end{cases} \quad (2)$$

With the change of switching combination as shown in Figure 3(b), the discharge interval of active boosting, the phase windings b and c are discharged into to battery source. The corresponding dynamics are given in (3).

$$Z_s = \begin{cases} Z_s \frac{di_{za}^{II}}{dt} = \frac{2V_{in} - V_B}{3} \\ Z_s \frac{di_{zb}^{II}}{dt} = \frac{-V_{in} + 2V_B}{3} \\ Z_s \frac{di_{zc}^{II}}{dt} = \frac{-V_{in} - V_B}{3} \end{cases} \quad (3)$$

With the change of switching combination as shown in Figure 3(c), the charging period of the active rectifier the phase windings charged with respective levels of input voltage. The corresponding dynamics are given in (4).

$$Z_s = \begin{cases} Z_s \frac{di_{za}^{III}}{dt} = \frac{2V_{in}}{3} \\ Z_s \frac{di_{zb}^{III}}{dt} = \frac{-V_{in}}{3} \\ Z_s \frac{di_{zc}^{III}}{dt} = \frac{-V_{in}}{3} \end{cases} \quad (4)$$

With the change of switching combination as shown in Figure 3(d), the second discharge period of the active rectifier which is the symmetrical opposite winding discharge, the phase windings B and C are discharged into to battery source. The corresponding dynamics are given in (5).

$$Z_s = \begin{cases} Z_s \frac{di_{Za}^V}{dt} = \frac{2V_{in}-V_B}{3} \\ Z_s \frac{di_{Zb}^V}{dt} = \frac{-V_{in}+2V_B}{3} \\ Z_s \frac{di_{Zc}^V}{dt} = \frac{-V_{in}-V_B}{3} \end{cases} \quad (5)$$

A similar mirror operation for the negative cycle of input voltage is depicted in Figures 3(e)-3(h) with respective dynamic equations provided from (6) to (9).

$$\begin{cases} Z_s \frac{di_{Za}^V}{dt} = \frac{-2V_{in}+V_B}{3} \\ Z_s \frac{di_{Zb}^V}{dt} = \frac{V_{in}+2V_B}{3} \\ Z_s \frac{di_{Zc}^V}{dt} = \frac{V_{in}-2V_B}{3} \end{cases} \quad (6)$$

$$\begin{cases} Z_s \frac{di_{Za}^W}{dt} = \frac{-2V_{in}+V_B}{3} \\ Z_s \frac{di_{Zb}^W}{dt} = \frac{V_{in}-2V_B}{3} \\ Z_s \frac{di_{Zc}^W}{dt} = \frac{V_{in}+V_B}{3} \end{cases} \quad (7)$$

$$\begin{cases} Z_s \frac{di_{Za}^X}{dt} = \frac{-2V_i}{3} \\ Z_s \frac{di_{Zb}^X}{dt} = \frac{V_m}{3} \\ Z_s \frac{di_{Zc}^X}{dt} = \frac{V_m}{3} \end{cases} \quad (8)$$

$$\begin{cases} Z_s \frac{di_{Za}^{III}}{dt} = \frac{-2V_{in}+2V_B}{3} \\ Z_s \frac{di_{Zb}^{III}}{dt} = \frac{V_{in}-V_B}{3} \\ Z_s \frac{di_{Zc}^{III}}{dt} = \frac{V_{in}-V_B}{3} \end{cases} \quad (9)$$

Now, the active rectifier with modulation index m and the boost operation with duty cycle D result in the steady state battery voltage to be (10).

$$\begin{cases} G = \frac{1}{1-D} \\ V_B = mV_m G \sin(\omega t) \end{cases} \quad (10)$$

The transfer function of the converter to design the closed-loop current controller is obtained as follows:
i) The instantaneous current in the capacitor and voltage across the inductor are given as (11) and (12); and
ii) Averaging the above instantaneous quantities, it is obtained as (13)-(17).

$$i_{C_sw} = \frac{-V_{o_sw}}{R} D + (i_{L_sw} + \frac{-V_{o_sw}}{R}) D^1 = C \frac{dV_{o_sw}}{dt} \quad (11)$$

$$V_{L_sw} = V_{s_sw} D + (V_{s_sw} - V_{o_sw}) D^1 = L \frac{di_{L_sw}}{dt} \quad (12)$$

$$C \left(\frac{dV_o}{dt} + \frac{dv_o}{dt} \right) = \frac{-V_o}{R} + I_L D^1 + \frac{-v_o}{R} + i_L D^1 - i_L d - I_L d \quad (13)$$

$$L \left(\frac{dI_L}{dt} + \frac{di_L}{dt} \right) = V_R - V_o D^1 + v_R - v_o D^1 + V_o d + v_o d \quad (14)$$

$$C \frac{dV_o}{dt} = \frac{-V_o}{R} + i_L (1 - D) - I_L D \quad (15)$$

$$L \frac{di_L}{dt} = v_R - v_o D^1 + V_o d \quad (16)$$

$$G_{id} = \frac{i_L}{d} = \frac{V_o}{L} \frac{s + \frac{V_o + I_L R D^1}{V_o R C}}{s^2 + \frac{1}{R C s} + \frac{D^{12}}{L C}} \quad (17)$$

The frequency response obtained for the converter transfer function provided in (17) is shown in Figure 4. This depicts the inherent stability of the converter. However, the phase margin is very narrow in this case. With PI current controller as in (18) results in the frequency response of the converter with improved phase margin. This necessitates for the reference current to be generated by the phase inductors as given in (19).

$$G_C(s) = k \frac{1+sT}{sT} \quad (18)$$

$$\frac{i_L}{i_L^*} = \frac{G_C G_{id}}{1 + G_C G_{id}} \quad (19)$$

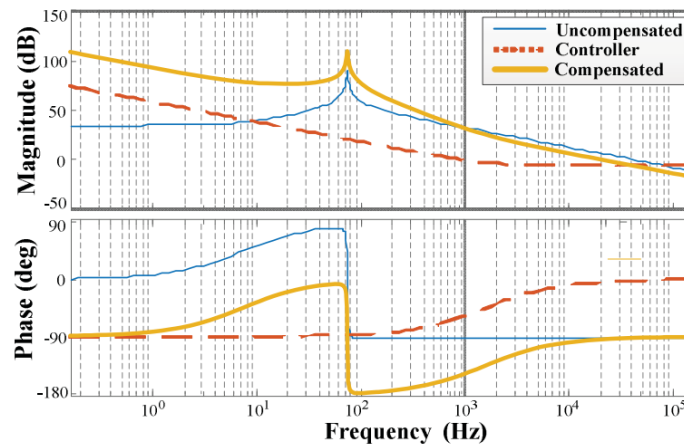


Figure 4. Frequency response for converter transfer function with and without controller

3. CONTROL OF THE DUAL FUNCTIONAL CONVERTER

The PI controller-based closed-loop control scheme for drive mode operation is shown in Figure 5. The sensed rotor speed is compared against the reference rotor speed. The error in rotor speed given to the PI controller determines the reference for the q-axis current. The reference for the d-axis current is made zero. The phase currents are sensed and converted into equivalent d-axis and q-axis components. The references obtained for q-axis and d-axis currents are compared against actual values. The error in each of the components given to PI controllers determines the instantaneous q-axis and d-axis voltage vectors respectively. The dq-abc transformation of these vectors provides instantaneous values for phase A, phase B, and phase C voltages. The sinusoidal pulse-width modulation (PWM) generates respective gating signals to generate instantaneous phase voltages.

The PI controller-based closed-loop control scheme for drive mode operation is shown in Figure 6. The sensed battery voltage is compared against the reference battery voltage. The error in rotor speed given to the PI controller determines the reference for phase current magnitude. Simultaneously the phase voltages are sensed and given to PLL to generate phase reference for each phase current. The reference for the d-axis current is made zero. The phase currents are sensed and converted into equivalent d-axis and q-axis components. The references obtained for q-axis and d-axis currents are compared against actual values. The error in each of the components given to PI controllers determines the instantaneous q-axis and d-axis voltage vectors respectively. The dq-abc transformation of these vectors provides instantaneous values for phase A, phase B, and phase C voltages. The sinusoidal PWM generates respective gating signals to generate instantaneous phase voltages.

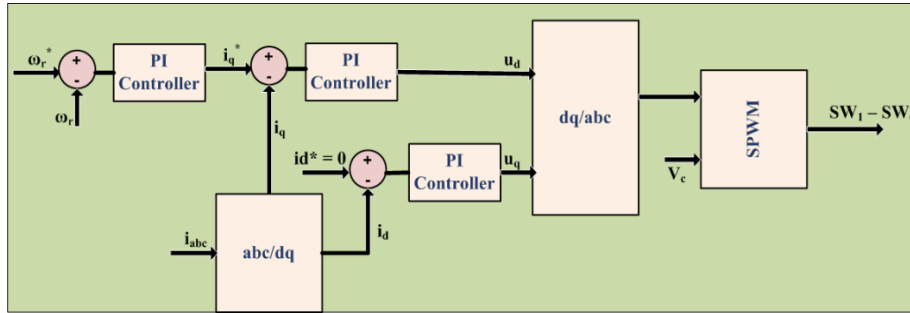


Figure 5. Control schematic for drive operation

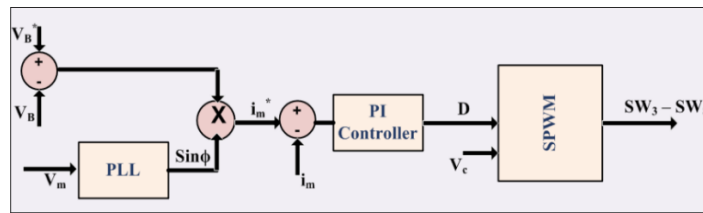


Figure 6. Control schematic for charging operation

4. SIMULATION RESULTS

The simulation of the proposed dual functional converter is carried out in MATLAB/Simulink. The simulation parameters for sources, load, and converter components are provided in Table 1. Simulation results for motor torque and speed for drive mode, input voltage and current, and battery voltage and current for charging mode are presented in this section.

Figure 7 presents the tracking of motor speed for a step change in speed command. A step change of 50 rpm is provided at 1 sec. The speed changed to a new set speed at 1.15 sec. The developed electromagnetic torque changing speed command is shown in Figure 8. The electromagnetic torque dips to the minimum value and settles to a new value for the changed speed requirement. The ripple in torque is obvious with the BLDC as seen in Figure 8. Further, the reverse motor operation is studied. A reverse speed command of 50 rpm is provided at 3 sec. The robustness of the PI controller is verified from the quick transient settlement of 0.15 sec as observed in Figure 9. The corresponding change in torque generated by the motor is depicted in Figure 10. Steady-state torque is depicted in Figure 11 which verifies the ripple in torque to be 2 N-m.

The charging operation is analyzed for input voltage, input current and battery side response along with inductor current. The unity power factor current drawn from the grid terminals is obtained as shown in Figure 12. Also, the voltage at first stage rectifier terminals is observed to be 230 V from Figure 13. Further, the battery bank voltage and current obtained verify the robustness of charging control. The phase windings acting as interfacing inductors also verify the design of phase winding for nominal switching frequency. The operational and structural characteristics of the drive such as component requirements, specialized construction of the motor, total harmonics distortions (THD). are compared to existing drives as depicted in Table 2. The comparison determines the effectiveness of economic aspects and reliability of the proposed drive.

Table 1. Simulation parameters

Parameter	Simulation
AC source	220 V, 50 Hz
Battery source	200 AH, $I_{max}= 20$ A, $V= 400$ V
K_p, K_i	0.0325, 0.224
BLDC specifications	10 kW, 20 N-m, 318 rad/sec, 4 Poles
Stator winding specifications	7.9 mΩ, 0.47 mH
Stator flux	104 mWb
Maximum current	30 A

Key observations:

- The developed DFPC exhibits better performance in mitigating input current ripple causing unity power factor and minimal THD input current drawn from the grid terminals.

- The dual functional control significantly reduced the THD to 0.8 percent, indicating a more sinusoidal and efficient current waveform in comparison to [19] and [21].
 The developed DFPC achieved an input current ripple comparable to the scheme using a specially designed motor [19]. However, the present design offers a simpler system structure by eliminating the need for such a motor.

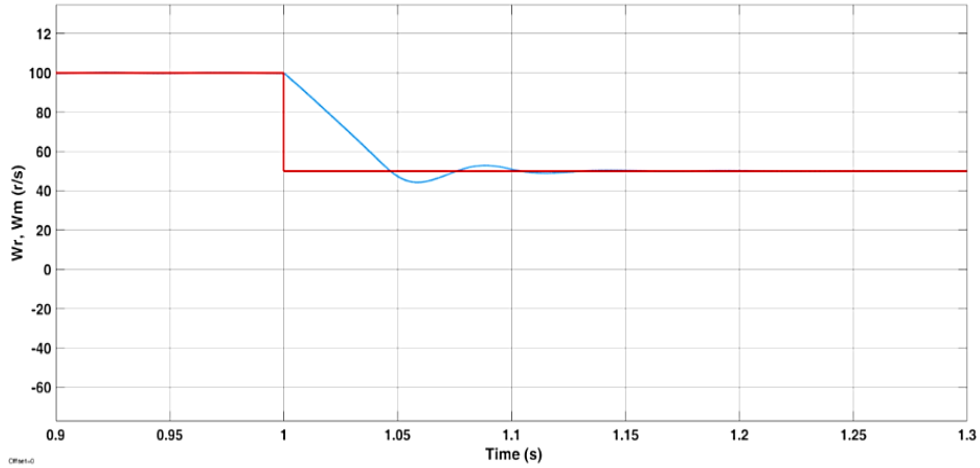


Figure 7. Speed response for step change in speed command

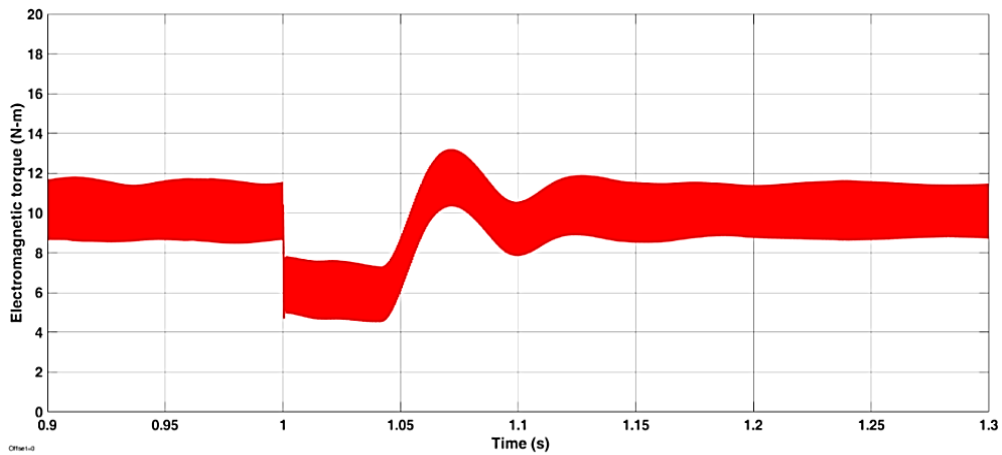


Figure 8. Electromagnetic torque response for a step change in speed

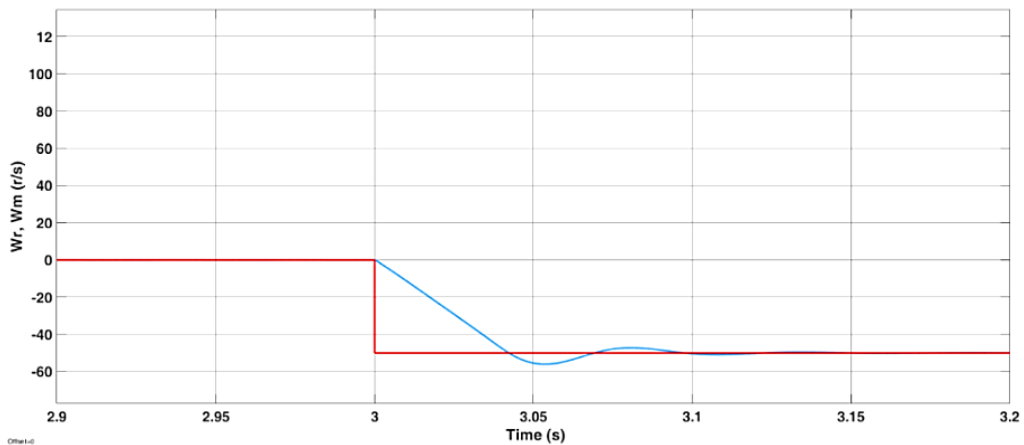


Figure 9. Speed response during transient speed reversal operation

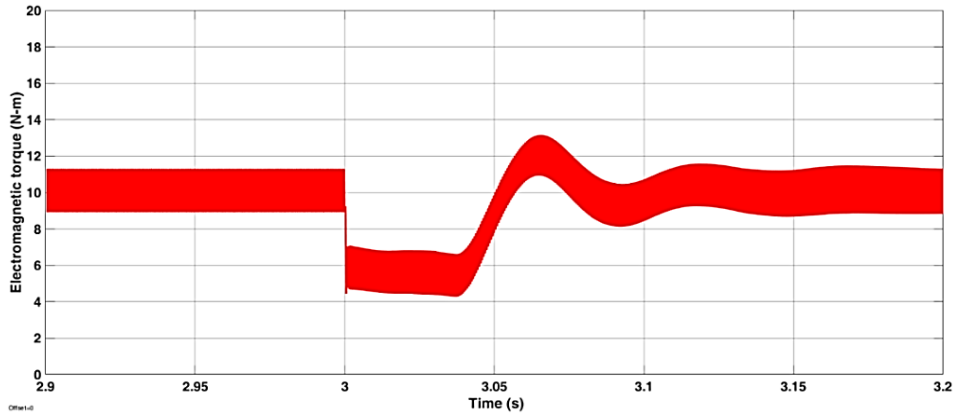


Figure 10. Electromagnetic torque response during speed reversal operation

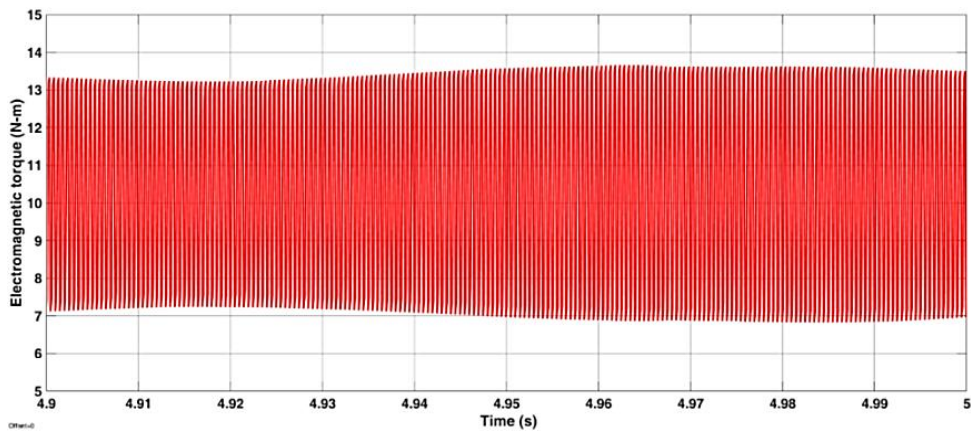


Figure 11. Steady-state torque

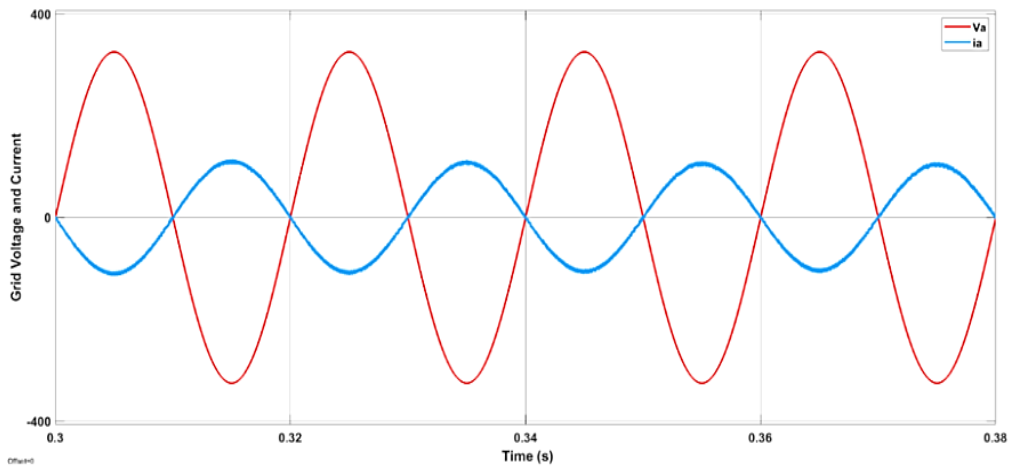


Figure 12. Grid voltage and current during the charging operation

Table 2. Comparison of proposed DFPC characteristics to existing drives

Drive topology	[14]	[19]	[21]	[27]	[28]	DFPC
Need for specialized motor	Yes	Yes	No	No	Yes	No
Requirement of auxiliary equipment	No	Yes	Yes	Yes	No	No
No. of switches	12	6	12	6	12	8
THD (%)	1.9	1.5	0.9	0.9	0.9	0.8
Battery current ripple (%)	5	5	5	2	2	1
Drive size normalized to proposed converter	2	1	2	1	1.5	1

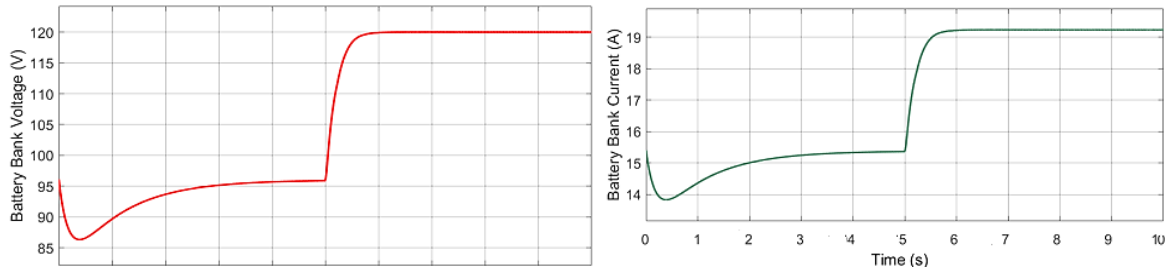


Figure 13. Battery voltage and battery current during charging operation

5. CONCLUSION

This paper presented a unified power converter for the drive and charge functions of BLDC-based electric vehicle drives. The symmetrical utilization of BLDC phase windings during charging operation is implemented for efficient power conversion. The unified converter operation, configuration, and control are presented. The proposed converter is simulated in the MATLAB/Simulink platform. The performance is evaluated in terms of operational variables such as voltage, current, torque, and speed. A comparative study is presented in terms of the size and efficiency of the proposed and existing drives. The proposed drive achieved 0.01 p.u. ripple in torque, 10 sec transient time for a change in speed full throttle command, and unity power factor current for charging operation which proved its robustness over the comparable drives.

FUNDING INFORMATION

Authors state no funding involved.

AUTHOR CONTRIBUTIONS STATEMENT

This journal uses the Contributor Roles Taxonomy (CRediT) to recognize individual author contributions, reduce authorship disputes, and facilitate collaboration.

Name of Author	C	M	So	Va	Fo	I	R	D	O	E	Vi	Su	P	Fu
Teja Sreenu Tadivaka	✓	✓		✓		✓		✓	✓	✓	✓	✓		✓
Malligunta Kiran Kumar	✓				✓		✓	✓		✓			✓	
Srungaram Ravi Teja		✓	✓		✓		✓		✓		✓	✓		✓
Ch. Rami Reddy	✓		✓	✓		✓		✓		✓	✓		✓	

- C : Conceptualization
- M : Methodology
- So : Software
- Va : Validation
- Fo : Formal analysis
- I : Investigation
- R : Resources
- D : Data Curation
- O : Writing - Original Draft
- E : Writing - Review & Editing
- Vi : Visualization
- Su : Supervision
- P : Project administration
- Fu : Funding acquisition

CONFLICT OF INTEREST STATEMENT

Authors state no conflict of interest.

DATA AVAILABILITY

Data availability is not applicable to this paper as no new data were created or analyzed in this study.

REFERENCES

[1] C. C. Chan, A. Bouscayrol, and K. Chen, "Electric, hybrid, and fuel-cell vehicles: Architectures and modeling," *IEEE Transactions on Vehicular Technology*, vol. 59, no. 2, pp. 589–598, 2010, doi: 10.1109/TVT.2009.2033605.

[2] S. Kumar and A. Usman, "A review of converter topologies for battery charging applications in plug-in hybrid electric vehicles," *2018 IEEE Industry Applications Society Annual Meeting, IAS 2018*, 2018, doi: 10.1109/IAS.2018.8544609.

- [3] F. Berthold, A. Ravey, B. Blunier, D. Bouquain, S. Williamson, and A. Miraoui, "Design and development of a smart control strategy for plug-in hybrid vehicles including vehicle-to-home functionality," *IEEE Transactions on Transportation Electrification*, vol. 1, no. 2, pp. 168–177, 2015, doi: 10.1109/TTE.2015.2426508.
- [4] A. Rezaei, J. B. Burl, M. Rezaei, and B. Zhou, "Catch energy saving opportunity in charge-depletion mode, a real-time controller for plug-in hybrid electric vehicles," *IEEE Transactions on Vehicular Technology*, vol. 67, no. 11, pp. 11234–11237, 2018, doi: 10.1109/TVT.2018.2866569.
- [5] F. Ahmadi, E. Adib, and M. Azari, "Soft switching bidirectional converter for reflex charger with minimum switches," *IEEE Transactions on Industrial Electronics*, vol. 67, no. 10, pp. 8355–8362, 2020, doi: 10.1109/TIE.2019.2947813.
- [6] U. Yilmaz, O. Turksay, and A. Teke, "Intelligent control of high energy efficient two-stage battery charger topology for electric vehicles," *Energy*, vol. 186, 2019, doi: 10.1016/j.energy.2019.07.155.
- [7] F. Yu, W. Zhang, Y. Shen, and J. Mao, "A nine-phase permanent magnet electric-drive-reconstructed onboard charger for electric vehicle," *IEEE Transactions on Energy Conversion*, vol. 33, no. 4, pp. 2091–2101, 2018, doi: 10.1109/TEC.2018.2844793.
- [8] M. Yilmaz and P. T. Krein, "Review of battery charger topologies, charging power levels, and infrastructure for plug-in electric and hybrid vehicles," *IEEE Transactions on Power Electronics*, vol. 28, no. 5, pp. 2151–2169, 2013, doi: 10.1109/TPEL.2012.2212917.
- [9] S. Haghbin *et al.*, "Integrated chargers for EV's and PHEV's: Examples and new solutions," *19th International Conference on Electrical Machines, ICEM 2010*, 2010, doi: 10.1109/ICELMACH.2010.5608152.
- [10] M. Grenier, M. G. H. Aghdam, and T. Thiringer, "Design of on-board charger for plug-in hybrid electric vehicle," *IET Conference Publications*, vol. 2010, no. 563 CP, 2010, doi: 10.1049/cp.2010.0101.
- [11] F. Naseri, E. Farjah, and T. Ghanbari, "An efficient regenerative braking system based on battery/supercapacitor for electric, hybrid, and plug-in hybrid electric vehicles with BLDC motor," *IEEE Transactions on Vehicular Technology*, vol. 66, no. 5, pp. 3724–3738, 2017, doi: 10.1109/TVT.2016.2611655.
- [12] M. Pushkarna *et al.*, "A new-fangled connection of UPQC tailored power device from wind farm to weak-grid," *Frontiers in Energy Research*, vol. 12, 2024, doi: 10.3389/fenrg.2024.1355867.
- [13] K. V. G. Rao *et al.*, "A new brushless DC motor driving resonant pole inverter optimized for batteries," *International Journal of Power Electronics and Drive Systems*, vol. 14, no. 4, pp. 2021–2031, 2023, doi: 10.11591/ijpeds.v14.i4.pp2021-2031.
- [14] R. Thapliyal, S. Bose, and P. Dwivedi, "An integrated bidirectional multi-source DC-DC converter with VMC approach for VSI-fed motor drive using non-isolated topology," *IEEE Transactions on Energy Conversion*, vol. 39, no. 2, pp. 1047–1058, 2024, doi: 10.1109/TEC.2023.3344039.
- [15] A. Furukawa, D. Graovac, T. Arai, and R. Vuletić, "A novel approach to affordable electric vehicles based on dual 48 V battery system with multi-functional 3-level converter," *PCIM Europe Conference Proceedings*, vol. 2024-June, pp. 305–314, 2024, doi: 10.30420/566262037.
- [16] A. K. Mishra and T. Kim, "An economical light plug-in electric vehicle (LPEV) with on-board single-stage battery charging system," *IEEE Transactions on Industry Applications*, vol. 59, no. 5, pp. 6568–6579, 2023, doi: 10.1109/TIA.2023.3285520.
- [17] J. Ye, C. Shi, and A. Khaligh, "Single-phase charging operation of a three-phase integrated onboard charger for electric vehicles," *2018 IEEE Transportation and Electrification Conference and Expo, ITEC 2018*, pp. 783–787, 2018, doi: 10.1109/ITEC.2018.8450212.
- [18] C. Shi, Y. Tang, and A. Khaligh, "A three-phase integrated onboard charger for plug-in electric vehicles," *IEEE Transactions on Power Electronics*, vol. 33, no. 6, pp. 4716–4725, 2018, doi: 10.1109/TPEL.2017.2727398.
- [19] F. Mahmouditabar, A. Vahedi, and N. Takorabet, "Robust design of BLDC motor considering driving cycle," *IEEE Transactions on Transportation Electrification*, vol. 10, no. 1, pp. 1414–1424, 2024, doi: 10.1109/TTE.2023.3285650.
- [20] M. Nagaraju and K. K. Malligunta, "Grid integration of hybrid renewable energy source using aligned multilevel inverter," *International Journal of Emerging Electric Power Systems*, vol. 23, no. 5, pp. 691–702, 2022, doi: 10.1515/ijeeps-2021-0366.
- [21] B. Saha, B. Singh, and A. Sen, "SMO based position sensorless BLDC motor drive employing canonical switching cell converter for light electric vehicle," *IEEE Transactions on Industry Applications*, vol. 59, no. 3, pp. 2974–2984, 2023, doi: 10.1109/TIA.2023.3241607.
- [22] P. Saiteja, B. Ashok, B. Mason, and P. S. Kumar, "Assessment of adaptive self-learning-based BLDC motor energy management controller in electric vehicles under real-world driving conditions for performance characteristics," *IEEE Access*, vol. 12, pp. 40325–40349, 2024, doi: 10.1109/ACCESS.2024.3375753.
- [23] B. Saha and B. Singh, "Adaptive delay signal cancellation- synchronous reference frame phase-locked loop based position sensorless single stage BLDC motor drive for light duty electric vehicle," *IEEE Transactions on Industry Applications*, vol. 60, no. 2, pp. 3229–3236, 2023, doi: 10.1109/TIA.2023.3348085.
- [24] G. Pellegrino, E. Armando, and P. Guglielmi, "An integral battery charger with power factor correction for electric scooter," *2009 IEEE International Electric Machines and Drives Conference, IEMDC '09*, pp. 661–668, 2009, doi: 10.1109/IEMDC.2009.5075276.
- [25] S. Sun, Q. Yang, and W. Yan, "A novel markov-based temporal-SoC analysis for characterizing PEV charging demand," *IEEE Transactions on Industrial Informatics*, vol. 14, no. 1, pp. 156–166, 2018, doi: 10.1109/TII.2017.2720694.
- [26] A. Rajeev V. and V. Prasad, "Online adaptive gain for passivity-based control for sensorless BLDC motor coupled with DC motor for EV application," *IEEE Transactions on Power Electronics*, vol. 38, no. 11, pp. 13625–13634, 2023, doi: 10.1109/TPEL.2023.3288939.
- [27] A. G. Cocconi, "Combined motor drive and battery recharge system," U.S. Patent 5 341 075A, Aug. 23, 1994.
- [28] Dong-Gyun Woo, G.-Y. Choe, J.-S. Kim, B.-K. Lee, Jin Hur, and Gu-Bae Kang, "Comparison of integrated battery chargers for plug-in hybrid electric vehicles: Topology and control," in *2011 IEEE International Electric Machines and Drives Conference (IEMDC)*, IEEE, May 2011, pp. 1294–1299. doi: 10.1109/IEMDC.2011.5994791.

APPENDIX

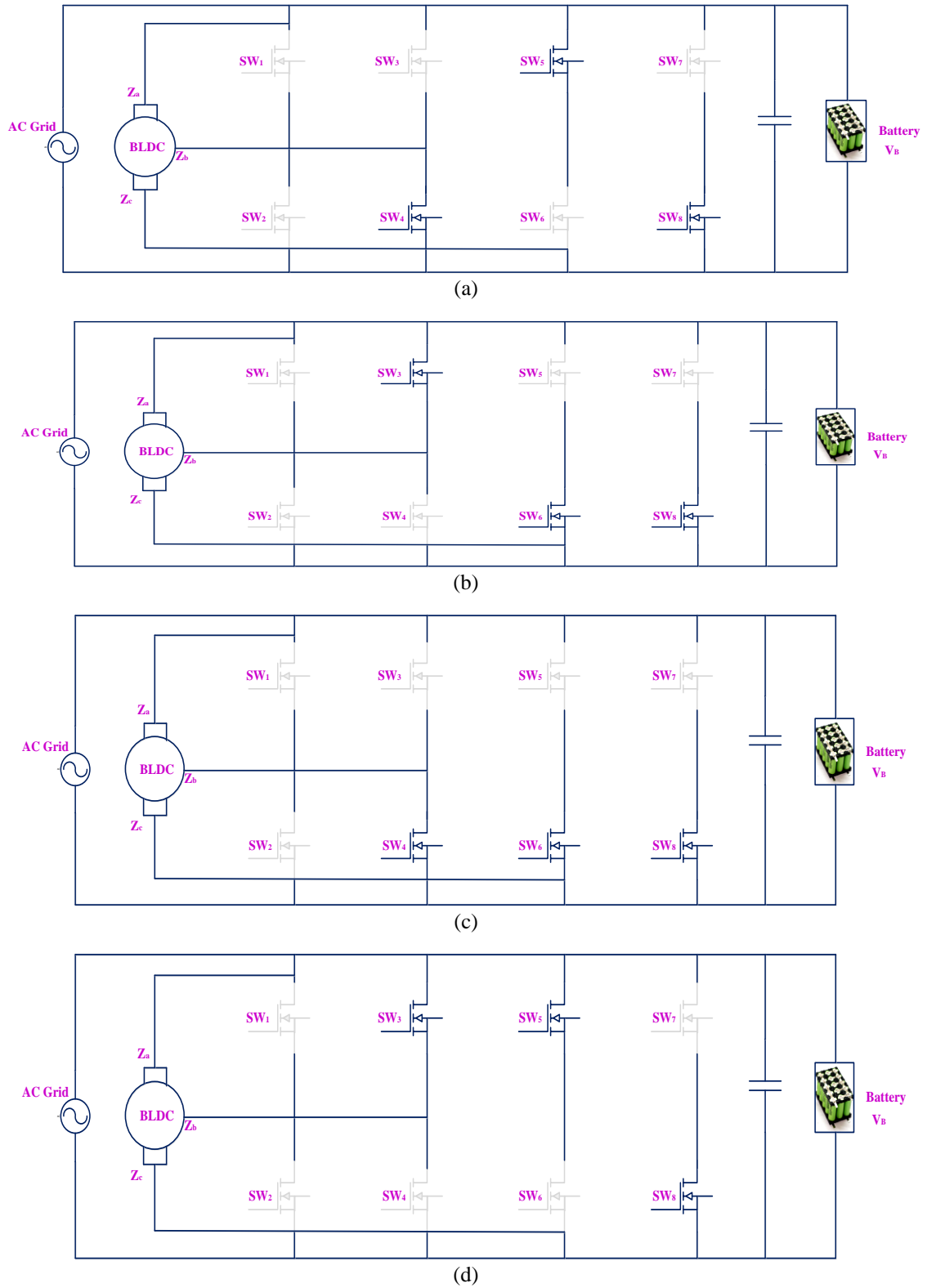
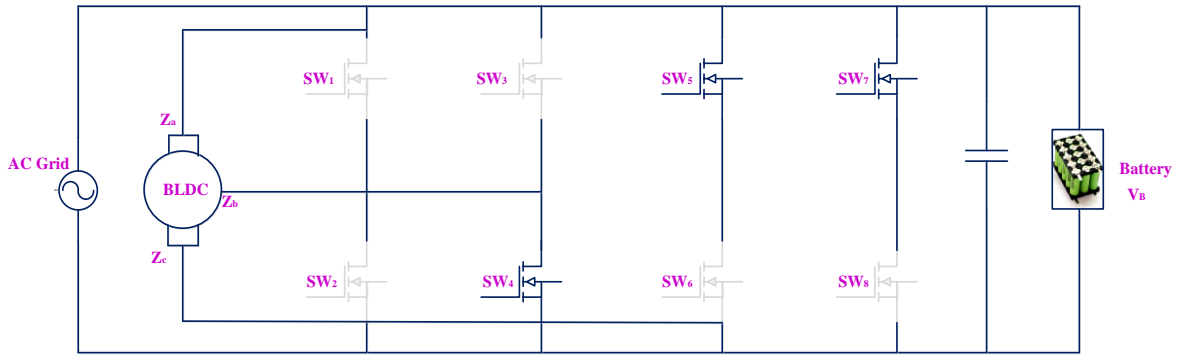
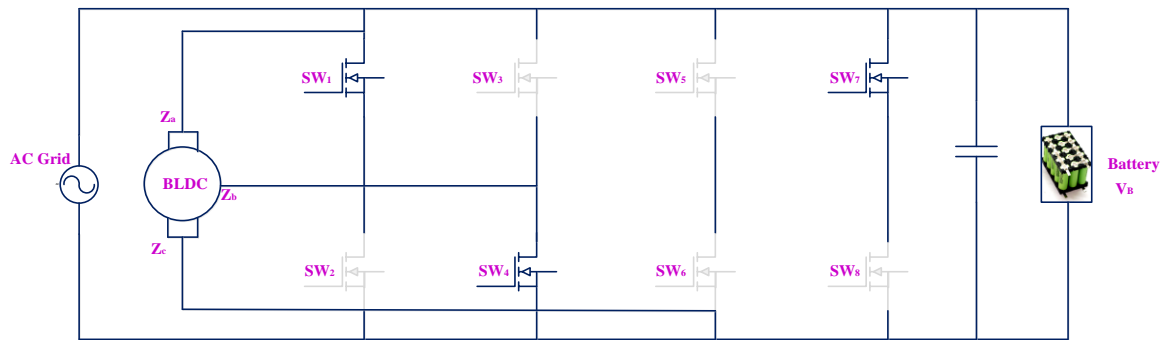


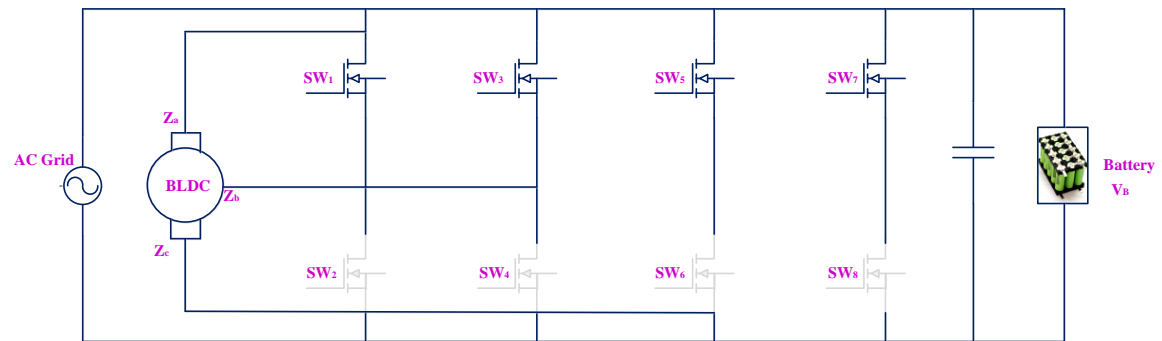
Figure 3. Charging mode switching sequence for dual functional converter: (a) active boost operation for +ve half cycle of input voltage, (b) phase B and phase C inductor discharging for +ve half cycle of input voltage, (c) phase inductors charging from AC source for +ve half cycle of input voltage, (d) second discharge into battery source for +ve half cycle of input voltage,



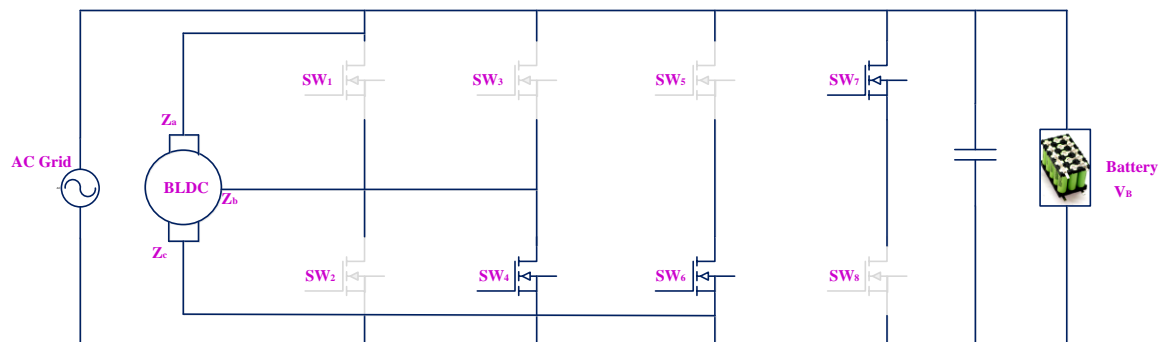
(e)



(f)






(g)






(h)

Figure 3. Charging mode switching sequence for dual functional converter: (e) phase b and phase c inductor discharging for -ve half cycle of input voltage, (f) active boost operation for -ve half cycle of input voltage, (g) phase inductors charging from AC source for -ve half cycle of input voltage, and (h) second discharge into battery source for +ve half cycle of input voltage (continued)




BIOGRAPHIES OF AUTHORS

Teja Sreenu Tadivaka    received the B.Tech. degree in Electrical and Electronics Engineering from JNTU Kakinada University in 2009, and the M.Tech. degree in Power and Industrial Drives from JNTU Kakinada University in 2011. Currently, he is a research scholar and assistant professor in the Electrical and Electronics Engineering Department at KL Deemed to be University, Guntur, AP, India. His research interests include power quality, fuel cell electric vehicle, electric vehicles, brushless DC electric motor control, DC-DC converters, power electronics, battery chargers, and harmonic distortion. He can be contacted at email: tejasreenu.tadivaka@gmail.com.






Malligunta Kiran Kumar    is working as an Associate Professor in the Department of Electrical and Electronics Engineering, Koneru Lakshmaiah Education Foundation (KL Deemed to be University) College of Engineering, has about 16 years of teaching experience. He received his B.Tech. degree in Electrical and Electronics Engineering with distinction from JNTU Hyderabad and M.E. degree in Power Electronics and Drives with distinction from Anna University, Chennai. He received a Ph.D. degree in Electrical and Electronics Engineering from KL Deemed to be University, Guntur, Andhra Pradesh. He has published more than 70 Scopus, SCI, and ESCI research papers in refereed international journals and 16 research papers in the proceedings of various international conferences, and three patents to his credit. He received the best teacher award five times, and his research interests include switched reluctance machines, power electronics, electric vehicles, and control systems. He is an active member of SIEEE, MISTE, and IEL. He can be contacted at email: kiran.malligunta@gmail.com.



Srungaram Ravi Teja    is Assistant Professor in the Electrical and Electronics Engineering Department at KL Deemed to be University, Guntur, AP, India. He received his B.Tech. degree in Electrical and Electronics Engineering from JNTUK in 2012, and M.Tech. degree in Electrical Engineering from NIT Warangal in 2015. His research interests include the field of power electronics, motor drives, renewable energy, FPGA applications, embedded systems, artificial intelligence, and intelligent control. He can be contacted at email: srungaramraviteja@gmail.com.



Ch. Rami Reddy    received B.Tech. degree in electrical and electronics engineering, M.Tech. degree in electrical machines and drives from Jawaharlal Nehru Technological University, Kakinada, Andhra Pradesh, in 2011, 2014 respectively and the Ph.D. degree in electrical and electronics engineering from K. L. University, Andhra Pradesh, India, in February 2022. He did a post-doctoral fellowship in electrical power systems from the National Institute of Technology, Srinagar, and Chonnam National University, South Korea. He is currently working as an associate professor in electrical and electronics engineering at Joginpally B R Engineering College, Hyderabad, India. His current research interests include integrated renewable energy systems, distributed generation, FACTS devices, power converters, and their applications to energy systems. He can be contacted at email: creddy229@gmail.com.